J Mol Model (2013) 19:4173–4180
DOI 10.1007/s00894-013-1794-z

ORIGINAL PAPER

Conformation-dependent conductance through a molecular break junction

Bartłomiej M. Szyja · Huu Chuong Nguyen · Daniel Kosov · Nikos L. Doltsinis

Received: 4 November 2012 / Accepted: 5 February 2013 / Published online: 27 February 2013

Abstract Ab initio molecular dynamics simulations have been performed of a gold—1,4-benzenedithiol (BDT)—gold nanojunction under mechanical stress. For three different pulling rates between 10 and 40 m s^{-1}, it is found that the nanowire always ruptures between the second and third Au atom from the thiol sulfur. Larger rupture forces and longer extensions are required at higher pulling rates and vice versa. The electrical conductance was calculated along a pulling trajectory using the DFT-NEGF method to study the effect of thermal and stress-induced structural changes on the electrical transport properties. While the mechanically induced stretching of the junction is seen to lower the time-averaged conductance, thermal conformational changes are capable of altering the conductance by one order of magnitude. No single geometric quantity could be identified as the main contributor to the conductance fluctuations. Small modulations, however, can be explained in terms of C=C double bond vibrations in the BDT molecule. The dependence of the conductance on different geometric variables has further been investigated systematically by performing constrained geometry optimizations along a number of angle and dihedral coordinates. The largest changes in the conductance are observed when the Au-S-C angle and the Au-S-C-C dihedral are simultaneously constrained.

B. M. Szyja (✉) · H. C. Nguyen · N. L. Doltsinis
Institute for Solid State Theory,
Department of Physics, University of Münster,
Wilhelm-Klemm Str. 10, 48149 Münster, Germany
e-mail: b.szyja@uni-muenster.de

D. Kosov
School of Engineering and Physical Science,
James Cook University, Townsville, Australia

Keywords Benzenedithiol · Conductance · External force · Gold · Nano-wire · Density functional theory · Non-equilibrium Green's function

Introduction

Understanding the electron transport properties of a molecule electrically wired to two electrodes is an important step toward building functional electronic devices based on single molecules, e.g., molecular transistors.

A widely used strategy to reliably wire a molecule to the electrodes is to attach the molecule with two appropriate terminal groups, such as thiols, that can bond covalently to the metal electrodes [1–9].

Two kinds of dithiol molecules have been extensively studied, one of which is the alkanedithiol chain. These molecules are considered highly insulating because of their large HOMO-LUMO gap, but they are relatively simple and chemically inert, which make them a nice model system to test an experimental technique or theoretical method [8]. The second group of these compounds are dithiols, based on conjugated aromatic oligomers, such as oligophenyldithiols and oligophenyleneethynylenedithiols [7]. The smaller HOMO-LUMO gap and the possibility of functionalizing these molecules make them more attractive for potential molecular electronics applications.

The simplest molecule of the latter group, benzenedithiol (BDT), has been investigated experimentally by scanning tunnelling microscopy (STM) [10–12] and break junction techniques [2]. Calculations of the conductance have been carried out using first principles simulations for the alkanedithiol [13] and give relatively good results compared to experiment differing by a factor of 3, while for benzenedithiol the disagreement is by a factor of 50 [14]. Despite such a big quantitative discrepancy, the simulations

are able to explain the relevance of the connection of the BDT molecule to the surface via additional Au atoms and its influence on the shape of the I-V curve.

Aim and scope of the study

Previous ab initio calculations have shown that mechanical stretching of thiol–gold contacts can result in monoatomic gold wires being pulled out of the gold electrodes [15, 16].

This idea has been corroborated in recent experiments in which an electric current was measured at pulling distances as large as 1 to 2 nm, i.e., much larger than the BDT molecule [8, 17].

The effect of the pulling, on the one hand, and the conformational dynamics, on the other, on the electrical conductance through BDT attached to one-dimensional gold wires, however, is still poorly understood.

In this study, the electrodes have the geometry of a 1-D gold chain that can be considered as already pulled out from the Au surface by the sulfur atoms, thus ignoring the surface itself. The emphasis of this work is clearly on unraveling the influence of conformational changes of the junction and the mechanical pulling on the conductance. The understanding gained could be a first step toward developing control mechanisms (e.g., switching on/off) over a molecular electronics device in the future, for instance by selectively exciting certain vibrational modes by infrared radiation.

As for the exact conductance value of Au-BDT-Au junctions, it is commonly believed that DFT considerably overestimates this quantity [18–20]. It has been suggested recently that the GW approximation yields quantitatively much more accurate results [19, 20]. However, there is also a wide spread in experimental results ranging from 10^{-4} to $0.5\,G_0$ (see [1] and references therein).

Model system and computational details

All ab initio molecular dynamics (MD) simulations were performed with the SIESTA code version 3.1 [21] using the PBE functional [22, 23], and DZP numerical basis set. The temperature was controlled by a Nosé thermostat [24] setting the average to 300 K.

The system consisted of a BDT molecule embedded in monoatomic gold chain of a total length of eight atoms, four on each side of the BDT molecule. Both ends of the chain were connected by applying periodic boundary conditions (unit cell dimensions: 13×13×25 Å ^{3}) thus forming a quasi-infinite wire.

For the MD simulation of the mechanical pulling we employed the following procedure: as the starting geometry for the MD run, we used the geometry optimized in the original simulation box of length 25 Å. After each 100 steps of 0.5 fs, i.e., the total time of 50 fs, the size of the box was increased by 0.01 Å in *z*-direction.

This amounts to a pulling speed of 20 m s^{-1}, which is low compared to other theoretical studies [1], but much faster than typical experimental pulling rates of 0.4–162.5 nm s^{-1} [25].

We ensured that atomic velocities were continuous between two pulling steps by always restarting the velocities from the previous run. This procedure was repeated until one of the bonds in the system was broken due to the external force. The rupture force was evaluated from the derivative of the system's total potential energy.

In order to study the influence of the pulling rate on the rupture force, we also carried out analogous simulations, with 200 and 50 steps in each consecutive run, resulting in pulling rates of 10 and 40 m s^{-1}.

The conductance of the junction was calculated for the 20 m s^{-1} run using the TranSIESTA extension to the SIESTA code [26] which allows electron transport calculations by combining non-equilibrium Green's functions (NEGF) with density functional theory (DFT). The core ideas of the DFT-NEGF implementation are described in [27]. All conductance values in this article have been multiplied by a factor of two as this is the default in TranSIESTA for non-spin-polarized calculations.

As in the MD runs, the PBE functional and DZP basis set were employed for the conductance calculations. The conductance calculations were carried out along the trajectory for the last geometries of each pulling step, i.e., every 0.01 Å, from 25.00 Å to 30.73 Å, where the chain has ruptured.

The electrodes were constructed as an ideal Au chain, with equal distance between the Au atoms (2.54 Å) attached to the outermost Au atoms from the pulling simulation. The *x* and *y* coordinates of the chain of the electrode have been set to the same values as the Au atom coupled to the electrode. The length of the electrodes was set to 11 atoms, as this yields the best convergence of the conductance results. Five gold atoms were defined as the bulk region and the remaining six gold atoms were added to the scattering region to screen out the perturbations in the scattering region.

The conductance G was calculated from the obtained transmission spectrum using the Fisher-Lee relation and the Landauer formula [28, 29] in the limit of low bias as

$$G = T\left(\in_F\right) G_0, \tag{1}$$

where $G_0 = 2e^2/h$ is the quantum of conductance and $\in_F$ is the Fermi energy. We have compared our results with a 3×3 atoms bulk surface and found that the results for the transmission spectrum at the Fermi level are comparable (give the same trend) with those obtained by the 1-D chain.

Results and discussion

Chain stretching and bond rupture

Initially, the system was optimized in the 25 Å box, which was sufficiently small to keep the gold chain in a relaxed configuration. The average distance between the Au atoms was 2.526 Å, and the angle between the Au atoms in the chain varied quite significantly from 119.6° to 157.8°. We could observe, that the BDT molecule was twisted, and the Au-S-C angles were approximately 120°. Moreover, on each side of the BDT molecule, two nearest Au atoms were aligned in a straight line. The optimized structure is shown in Fig. 1a.

The first symptoms of bond breaking were observed at 29.4 Å. At this point the average length of the Au-Au bond increased to 2.75 Å, and the Au-Au-Au angles straightened up varying only slightly from 159° to 170° (see Fig. 1b). The two closest Au atoms (Au^9-Au^{10} and Au^{13}-Au^{14}, respectively) were no longer aligned along a straight line, as there is too much strain in the system.

Despite the formal symmetry of the system, pulling-induced bond breaking only occurs on one side of the BDT molecule. At a pulling distance of 29.5 Å, the Au^{14}-Au^{15} bond (see Fig. 1) chain was longer (3.02 Å) than Au^{10}-Au^{11} (2.61 Å). Therefore one would intuitively expect the former to break first. However, at 29.6 Å, the Au^{10}-Au^{11} distance increased to 3.1 Å, while the remaining bonds on the right hand side shrunk to the length of approximately 2.6 Å. This finally resulted in the rupture of the Au^{10}-Au^{11} bond, while the Au^{14}-Au^{15} bond shrunk back to a length of 2.63 Å.

The bond rupture was a symmetry-breaking event which left two Au atoms connected to the right side of BDT molecule, while the remaining six Au atoms formed a cluster on the left side (see Fig. 1c). Interestingly, out of the seven Au-Au bonds initially present in the system, the Au^{10}-Au^{11} bond appears to be the weakest one, independent of the pulling rate. After the rupture of the chain, the two gold atoms on the right closest to the BDT molecule again form a straight line with the sulfur atom. What is even more remarkable is the fact that the gold cluster on the left hand side of the BDT molecule also contains this part composed of a straight S-Au-Au configuration.

The external force necessary to break the gold chain was calculated using the formula:

$$F = -\frac{dE}{dz}, \tag{2}$$

where E is the potential energy of the system and z is the length of the periodic box in z-direction. Due to the relatively small number of MD steps for each pulling distance, the averaged potential energy curve (see Fig. 2, top panel) displays some local fluctuations. Prior to taking the derivative (2), we therefore fitted a quadratic function up to a z-length of 29.5 Å, just before the bond rupture point.

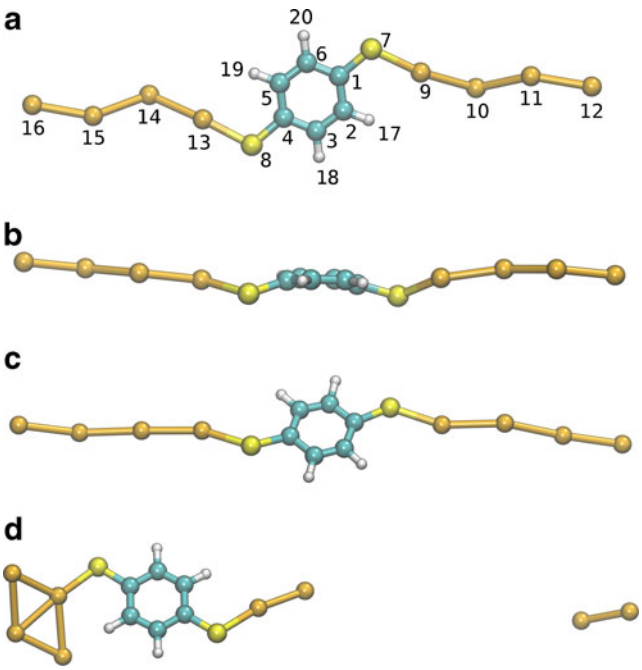

Fig. 1 **a** Optimized geometry at 25.00 Å. **b** snapshot of the out of plane distorted structure at 26.76 Å. **c** snapshot of a stretched geometry taken at 29.40 Å. **d** snaphot at 30.24 Å, after the Au-Au bond was broken

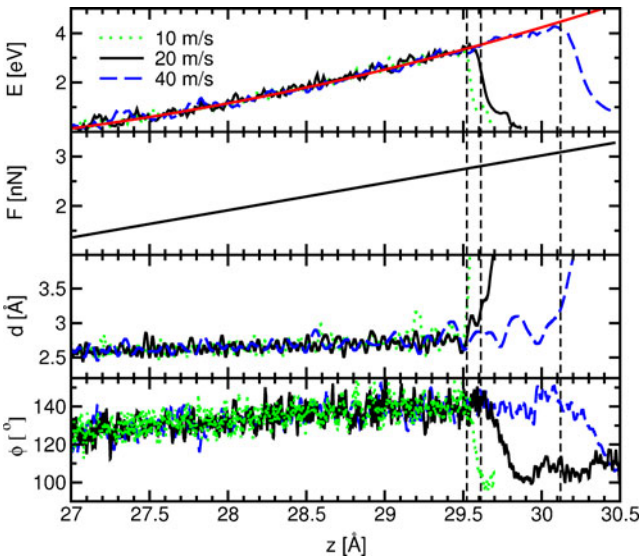

Fig. 2 *Top panel*: potential energy as a function of box length z for pulling speeds 10 m s^{-1} (*green dotted line*), 20 m s^{-1} (*black solid line*), 40 m s^{-1} (*blue dashed line*) and quadratic fit (*red solid line*). *Second panel*: absolute force calculated from the derivative of the quadratic fit. *Third panel*: Au^{10}-Au^{11} bond length, *d*. *Bottom panel*: C^1-S^7-Au^9 angle, ϕ. The *vertical dashed lines* indicate when the bond length *d* reaches 3.2 Å, i.e., the rupture point

As shown in the second panel of Fig. 2, the rupture force increases with the pulling speed from 2.8 nN for 10 m s^{-1} to 3.0 nN for 40 m s^{-1}. These values are greater than experimentally measured values of the Au-Au rupture force [30–33]. For single Au-thiol contacts, a force of 1.4 nN has been measured [30, 31]. When comparing our theoretical results with experimental values it is important to remember that the pulling rates in our simulations were several orders of magniture faster than the experimental ones.

From the trend observed in our simulations, the rupture force is expected to decrease significantly if the pulling rate is further decreased. However, it is impossible to extrapolate to experimental pulling rates based on the three values obtained here. Moreover, we need to bear in mind that a reliable result for the rupture force at a particular pulling rate requires averaging over a number of trajectories with different initial conditions.

It should be noted that a rupture of 1.5 nN, very similar to the experimental value, was obtained in a previous ab initio study [15, 16]. However, in these calculations a different pulling protocol, consisting of a combination of geometry optimizations and MD, was employed which does not permit the determination of a pulling rate but would certainly mimick much slower pulling than otherwise feasible by pure MD.

The third panel of Fig. 2, the Au^{10}-Au^{11} distance, *d*, is shown for the three trajectories. It can be seen that at advanced pulling stages, there are large oscillations in *d*; values above 3 Å are reached without breaking the bond. According to this observation, we consider the bond to be broken when the threshold of 3.2 Å is crossed.

The size of the box corresponding to the bond rupture is 29.5 Å for the 10 m s^{-1} pulling rate, 29.6 Å for 20 m s^{-1} and 30.1 Å for 40 m s^{-1}. In all cases the mechanism of bond breaking is the same, the bond connecting the two closest Au atoms on the left or on the right side of the BDT is elongated while the other Au-Au bonds shrink slightly. Subsequently, the bond is broken, and the structure analogous to one shown in Fig. 1c is formed.

The above trend, i.e., that faster pulling results in later rupture, has also been shown experimentally by Huang et al. [25]. The reason for this counter-intuitive behavior could be the following: The optimal geometric position for the C^1-S^7-Au^9 angle is around 105° as in Fig. 1c. This causes the gold chain to bend, leading to Au^9-Au^{10}-Au^{11} and Au^{13}-Au^{14}-Au^{15} angles smaller than 180°. The gold chain therefore adopts a zig-zag shape, which is not geometrically optimal, and breaks upon stretching. When the system is pulled at a faster rate, the C^1-S^7-Au^9 angle is opened wider allowing the gold chain to straighten up, and therefore the system becomes slightly longer before it actually breaks. The evolution of the C^1-S^7-Au^9 angle is shown in the bottom panel of Fig. 2.

Conductance calculations

Along the trajectory with a pulling speed of 20 m s^{-1}, we have calculated the conductance of the junction using the DFT-NEGF method. One should keep in mind that the DFT-NEGF assumes that the system is in a steady state and that it would have enough time to relax. Our NEGF calculations consider each trajectory snapshot separately and thus do not take into account the time or pulling speed.

The conductance calculated along the trajectory is shown in Fig. 3 (top panel). We can observe large variations in the conductance in the course of the trajectory. Initially it varies between 1.0 and 1.5 G_0, and reaches values above 1.5 G_0 for box sizes of approximately 26–28 Å. For this period we also observe smaller fluctuations in the conductance. This is followed by the period of decreased conductance up to approximately 29 Å. Just before the bond is broken, we observe very low conductance with only small fluctuations around 0.2–0.3 G_0. Finally, the conductance vanishes as the Au-Au bond ruptures.

A drop in conductance by more than two orders of magnitude upon stretching by 2.2 Å was observed in classical MD simulations of BDT connected to 3D gold electrodes in combination with an extended Hückel model for electron transport [34].

An important observation is that the conductance curve is not smooth with only small fluctuations, as we might have expected. Instead, the changes we observe are rather large and sudden. Therefore we need to assume the conductance of the system changes very rapidly due to geometric fluctuations, as there are no other factors present that could influence the conductance.

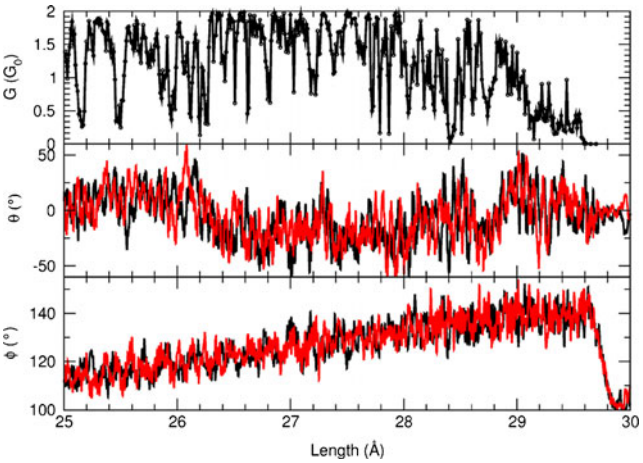

Fig. 3 *Top panel*: conductance change along the trajectory. *Middle panel*: left (*black*) and right (*red*) C-C-S-Au dihedral. *Bottom panel*: left (*black*) and right (*red*) C-S-Au angle

Figure 4 shows a conductance histogram obtained by averaging over two independent trajectories with different initial conditions at a pulling speed of 20 m s^{-1}. It is safe to conclude that the distribution is very broad, assuming values between 0 and $2G_0$. Any statement regarding possible peaks would need to be backed up by better statistics, i.e., a larger number of trajectories, which is beyond the scope of this article. Please note that the counts near zero conductance are for configurations after the bond rupture event. A broad distribution is consistent with the predictions by Andrews et al. [34] from classical simulations.

The evolution of a selection of Kohn-Sham orbitals in the vicinity of the Fermi level is shown in Fig. 5. The question is whether it is possible to rationalize the variations in the conductance in terms of orbital energies. We observe that the LUMO energy (red line) remains roughly constant, while the HOMO energy (black line) gradually increases during the pulling process up to the rupture point D. The narrowing of the HOMO–LUMO gap is, however, overcompensated by the decreasing energies of HOMO–1 to HOMO–4 (see Fig. 5) explaining the decrease in conductance as the wire is stretched (Fig. 3).

Can we deduct from the shape of the orbitals whether a particular conformation exhibits high or low conductance? Figure 6 depicts the HOMO–1, HOMO, and LUMO for the high conductance geometry A (z = 27.84 Å, $G = 1.88G_0$) and the neighboring low conductance geometry B (z = 27.87 Å, $G = 0.16G_0$). Despite the hugely different conductance values, the differences in the orbital shapes are rather subtle. Most notably, for the HOMO of B the BDT molecule appears to be drained of electron density, and the HOMO–1 shows more nodes than for A, making this channel less efficient.

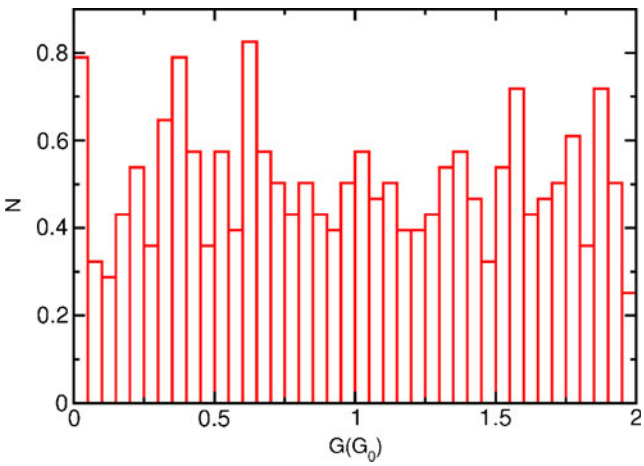

Fig. 4 Conductance histogram averaged over two trajectories at a pulling speed of 20 m s^{-1} with different initial conditions

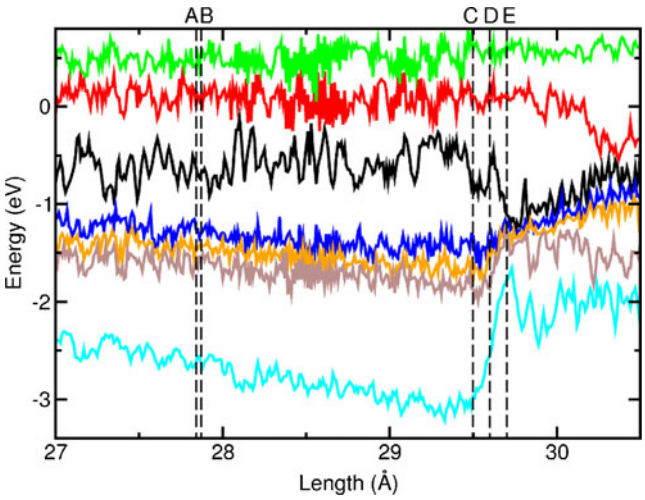

Fig. 5 Kohn-Sham orbital energies for the five highest occupied and two lowest unoccupied molecular orbitals. The electronic structure at points A–E is analyzed in more detail in Fig. 6

Figure 6c–e shows the orbitals at a point just before (C), during (D), and after (E) bond rupture. Our motivation for analyzing the electronic structure at those points was to see whether, for instance, the population of a particular antibonding orbital is responsible for triggering bond dissociation. As is apparent from Fig. 6, there is no obvious answer. The order and the character of the orbitals remain unchanged throughout the trajectory. In particular, the HOMO and HOMO–1 are both antibonding along the rupturing bond (between the second and third Au atom from the left). Compared to points A and B, the HOMO–1 has significantly less charge density on the gold chain, which might contribute to the dissociation.

To investigate in more detail the origin of the conductance fluctuations, we also searched for possible correlations between geometric changes and conductance variations. As the total amount of data is rather overwhelming, we decided to focus our analysis on selected characteristic sections of the conductance plot.

The first section is for box lengths between 27.43 Å and 27.44 Å. It is special, because the dihedral angles do not change much here and therefore the possible contributions to the conductance can be narrowed down considerably. First of all we looked at the C-C bond vibrations. Each C-C bond in the aromatic ring vibrates in its own phase, and their influence on the conductance (if any) must be different. Figure 7 shows the dihedrals (top panel) together with average C-C bond lengths (middle panel) and the conductance (bottom panel). Although to some extent there is correlation between the total average C-C length, the average value of the C^5-C^6 and C^2-C^3 bond lengths is seen to match even better. We can attribute this effect to the π-bonds

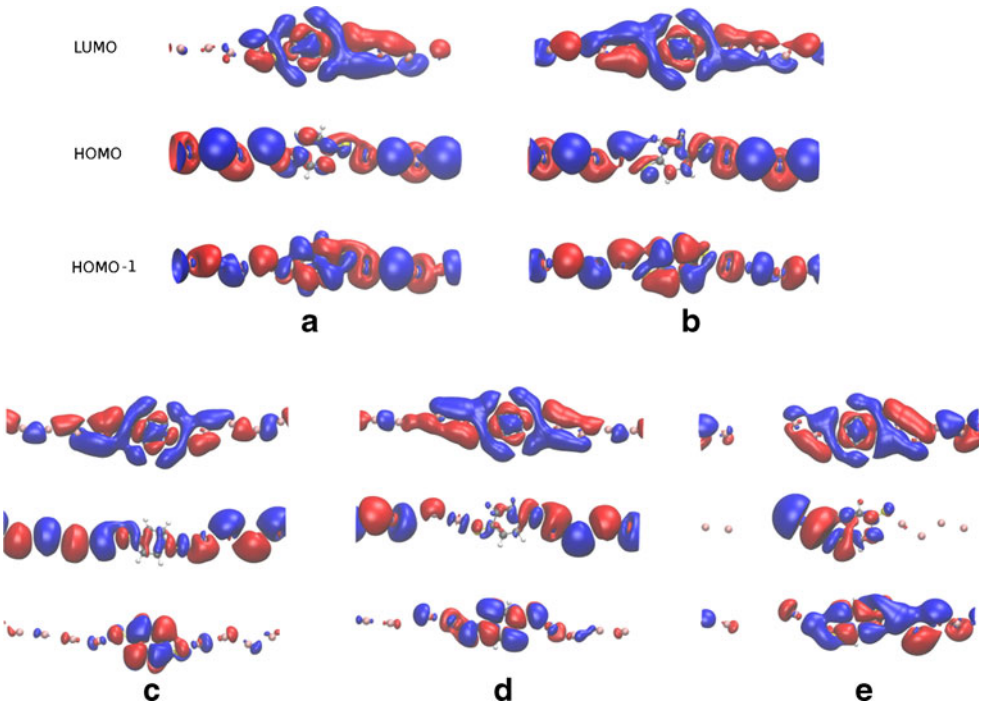

Fig. 6 Isosurface representation of Kohn-Sham orbitals HOMO–1, HOMO, and LUMO at geometries A–E as defined in Fig. 5

between the C-C, a mechanism that has been discussed previously in the literature [34–36].

However, the variations in the conductance in this particular section are minor. Hence we cannot explain the big and sudden conductance drops we observe during the total run by only vibrations of the C-C bonds.

To study the dependence of the conductance on geometric variables more systematically and to find additional correlations, we carried out two series of constrained geometry optimizations. In one series the angle formed by the Au-S-C atoms was varied between 90 and 180°. In another series, the dihedral angle formed by the Au-S-C-C atoms was scanned between 0 and 180°. This set of constraints was chosen due to the fact that the changes in the geometry in the 1-D Au chain are minor, and we expect the predominant influence on the conductance to be from the BDT molecule itself and the Au-BDT interface. The angle and the dihedral scans were performed for the 27 Å box length, because it displays a high conductance, and therefore we expected any changes to be amplified and thus more easily observable.

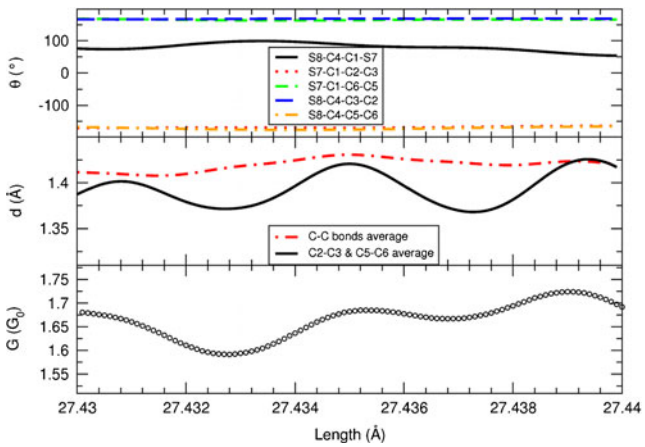

Fig. 7 Dihedral angles (*top panel*), C-C bond averages (*middle panel*) and conductance (*bottom panel*) between 27.43 Å and 27.44 Å

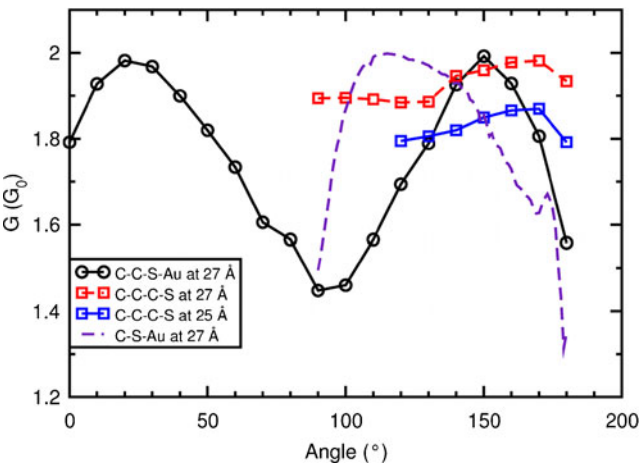

Fig. 8 Conductance of singly constrained geometries at a *z* length of 27 Å (*black*: C^6-C^1-S^7-Au^9 dihedral, *red*: C^5-C^6-C^1-S^7 dihedral, *purple*: C^1-S^7-Au^9 angle) and 25 Å (*blue*: C^5-C^6-C^1-S^7 dihedral), respectively

The changes in the conductance with respect to the constraints are shown in Fig. 8. Although relatively large changes can be seen for the C-C-S-Au dihedral and C-S-Au angle curves, their magnitude is still too small to explain the very low values occuring over the trajectory.

We only observe differences in the conductance of less than 40 % compared to the optimized geometry, whereas the changes reaching 80 % are observed in the MD run. Therefore, we conclude that a concerted motion of several geometric quantities is necessary to induce the extreme changes in the conductance seen in the trajectory.

For this reason, we performed additional geometry optimizations with two degrees of freedom constrained, namely the Au-S-C angle and the Au-S-C-C dihedral.

Note that these are the same constraints as described above, except this time both angle and dihedral were constrained at the same time. We also changed the range of the scan to better match the range observed in the trajectory. The results are shown in Fig. 9.

The conductance changes in the plot from approx 0.5 to $1.8\,G_0$. This can explain the significant changes in the conductance during the MD trajectory. The plot allows us to draw more general conclusions as well.

For smaller values of the Au-S-C-C dihedral angle we can observe better conductance, while larger dihedrals are seen to lower the conductance. The energetic minimum for this dihedral, lies in the 10–20° range, i.e., in the high conductance region.

The energetic minimum of the Au-S-C angle (at approximately 125°) also corresponds to a maximum of conductance. However the situation is reversed when the dihedral angle increases, and we observe better conductance for the angle of 105°.

This observation has two implications. Firstly, the system in relaxed configuration displays good conductance. But secondly, it shows how moderate geometric changes can significantly change the conductance. Furthermore, it is important to realize that in these doubly constrained optimizations, only one side of the Au-BDT-Au junction is fixed, while the other is free to relax. The effects seen in Fig. 9 are expected to be amplified if both sides are constrained simultaneously.

Although it would be theoretically possible to carry out such quadruply constrained optimizations, this is beyond the scope of the present paper.

Conclusions

We have performed ab initio molecular dynamics simulations of a BDT molecule embedded in a one-dimensional gold chain at different pulling rates. In all cases, the gold chain was broken in the same place. However, rupture was seen to occur later for faster pulling speeds.

For the trajectory with a 20 m s^{-1} pulling rate, we have computed the conductance as a time-dependent signal along the run.

It was attempted to correlate the dynamical conductance fluctuations observed with geometric quantities. Minor modulations have been found to be due to C-C bond vibrations in the π-system of BDT.

Systematic investigations of the influence of geometric parameters on the conductance have been carried out by scanning selected bond and dihedral angles in constrained geometry optimizations.

We conclude that the observed large fluctuations in the conductance cannot be explained simply by a single parameter.

We have obtained evidence through doubly constrained geometry optimizations that simultaneous changes in the Au-S-C angle and Au-S-C-C dihedral can have a major impact on the conductance. To fully explain the observed conductance time signal, however, a concerted motion of multiple degrees of freedom is necessary.

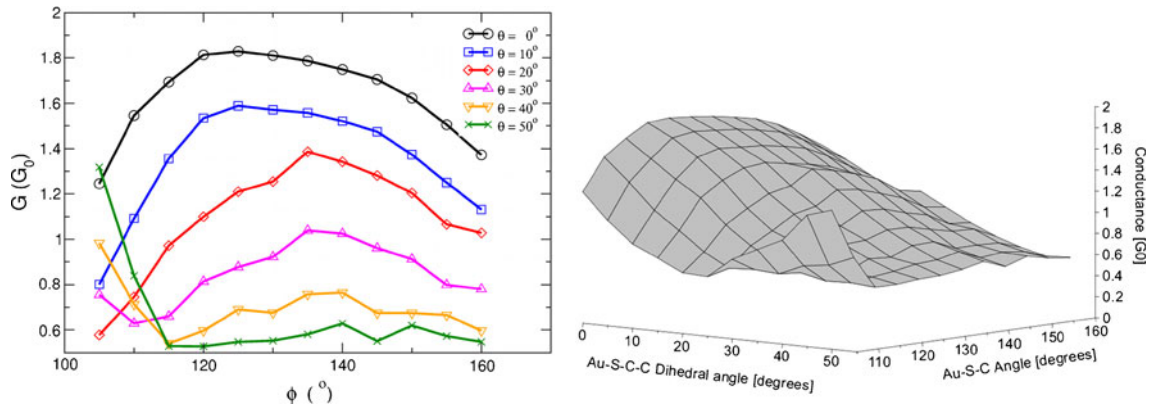

Fig. 9 Conductance of double constrained geometries in a 2-D (*left*) and 3-D (*right*) representation

References

1. Hakkinen H (2012) Nature Chem 4(6):443. doi:10.1038/nchem.1352
2. Reed MA, Zhou C, Muller CJ, Burgin TP, Tour JM (1997) Science 278(5336):252. doi:10.1126/science.278.5336.252
3. Park J, Pasupathy AN, Goldsmith JI, Chang C, Yaish Y, Petta JR, Rinkoski M, Sethna JP, Abruna HD, Mceuen PL, Ralph DC (2002) Nature 417(6890):722. doi:10.1038/nature00791
4. Reichert J, Ochs R, Beckmann D, Weber HB, Mayor M, Löhneysen (2002) Phys Rev Lett 88(17):176804. doi:10.1103/PhysRevLett.88.176804
5. Liang W, Shores MP, Bockrath M, Long JR, Park H (2002) Nature 417(6890):725. doi:10.1038/nature00790
6. Cui XD, Primak A, Zarate X, Tomfohr J, Sankey OF, Moore AL, Moore TA, Gust D, Harris G, Lindsay SM (2001) Science 294(5542):571. doi:10.1126/science.1064354
7. Kushmerick JG, Holt DB, Yang JC, Naciri J, Moore MH, Shashidhar R (2002) Phys Rev Lett 89(8):086802+. doi:10.1103/PhysRevLett.89.086802
8. Xu B, Tao NJ (2003) Science 301(5637):1221. doi:10.1126/science.1087481
9. Smit RHM, Noat Y, Untiedt C, Lang ND, van Hemert MC, van Ruitenbeek JM (2002) Nature 419(6910):906. doi:10.1038/nature01103
10. Dorogi M, Gomez J, Osifchin R, Andres RP, Reifenberger R (1995) Phys Rev B 52:9071. doi:10.1103/PhysRevB.52.9071
11. Andres RP, Bein T, Dorogi M, Feng S, Henderson JI, Kubiak CP, Mahoney W, Osifchin RG, Reifenberger R (1996) Science 272(5266):1323. doi:10.1126/science.272.5266.1323
12. Xiao X, Tao NJ (2004) Nano Lett 4(2):267. doi:10.1021/nl035000m
13. Tomfohr JK, Sankey OF (2002) Phys Stat Sol b 233(1):59. doi:10.1002/1521-3951(200209)
14. Tomfohr J, Sankey OF (2004) J Chem Phys 120(3):1542. doi:10.1063/1.1625911
15. Krüger D, Fuchs H, Rousseau R, Marx D, Parrinello M (2002) Phys Rev Lett 89(18):186402
16. Krüger D, Rousseau R, Fuchs H, Marx D (2003) Angew Chem Int Ed 42:2251
17. Reddy P, Jang SY, Segalman RA, Majumdar A (2007) Science 315(5818):1568. doi:10.1126/science.1137149
18. Borges Pontes R, Rocha AR, Sanvito S, Fazzio A, da Silva AJR (2011) ACS Nano 2:795
19. Strange M, Rostgaard C, Häkkinen H, Thygesen KS (2011) Phys Rev B 83:115108
20. Strange M, Thygesen KS (2011) Beilstein J Nanotechnol 2:746
21. Soler JM, Artacho E, Gale JD, García A, Junquera J, Ordejón P, Daniel NO (2002) J Phys Cond Matt 14(11):2745. doi:10.1088/0953-8984/14/11/302
22. Perdew JP, Burke K, Ernzerhof M (1996) Phys Rev Lett 77(18):3865. doi:10.1103/PhysRevLett.77.3865
23. Perdew JP, Burke K, Ernzerhof M (1997) Phys Rev Lett 78(7):1396. doi:10.1103/PhysRevLett.78
24. Nosé S (1984) J Chem Phys 81(1):511. doi:10.1063/1.447334
25. Huang F, Chen PA, Bennett T (2007) J Am Chem Soc 129(43):13225. doi:10.1021/ja074456t
26. Brandbyge M, Mozos JL, Ordejón P, Taylor J, Stokbro K (2002) Phys Rev B 65:165401. doi:10.1103/PhysRevB.65.165401
27. Xue Y, Datta S, Ratner MA (2002) Chem Phys 151(2â€“3). doi:10.1016/S0301-0104(02)00446-9
28. Fisher DS, Lee PA (1981) Phys Rev B 23:6851. doi:10.1103/PhysRevB.23.6851
29. Büttiker M, Imry Y, Landauer R, Pinhas S (1985) Phys Rev B 31:6207. doi:10.1103/PhysRevB.31.6207
30. Grandbois M, Beyer M, Rief M, Clausen-Schaumann H, Gaub HE (1999) Science 283:1727
31. Xu BQ, Xiao YX, Tao JN (2003) J Am Chem Soc 125:16164
32. Pu Q, Leng Y, Zhao X, Cummings PT (2010) J Phys Chem C 114(23):10365. doi:10.1021/jp101689u
33. Frei M, Aradhya SV, Koentopp M, Hybertsen MS, Venkataraman L (2011) Nano Lett 11(4):1518. doi:10.1021/nl1042903
34. Andrews DQ, Van Duyne RP, Ratner MA (2008) Nano Lett 8:1120
35. Chen W, Widawsky JR, Vásquez H, Schneebeli ST, Hybertsen MS, Breslow R, Venkataraman L (2011) J Am Chem Soc 133:17160
36. Diez-Perez I, Hihath J, Hines T, Wang ZS, Zhou G, Müllen K, Tao N (2011) Nature Nanotech 6(4):226. doi:10.1038/nnano.2011.20